

Article

Analysis of Motile Gyrotactic Micro-Organisms for the Bioconvection Peristaltic Flow of Carreau–Yasuda Bionanomaterials

Zahid Nisar ^{1,*}  and Humaira Yasmin ^{2,*} 

¹ Department of Computer Science, National University of Sciences and Technology (NUST), Balochistan Campus (NBC), Quetta 87300, Pakistan

² Department of Basic Sciences, Preparatory Year Deanship, King Faisal University, Al-Ahsa 31982, Saudi Arabia

* Correspondence: zahidnisar@nbc.nust.edu.pk (Z.N.); hhassain@kfu.edu.sa or qau2011@gmail.com (H.Y.)

Abstract: Nanofluids are considered as an effective way to enhance the thermal conductivity of heat transfer fluids. Additionally, the involvement of micro-organisms makes the liquid more stable, which is important in nanotechnology, bio-nano cooling systems, and bio-microsystems. Therefore, the current investigation focused on the examination of the thermodynamic and mass transfer of a Carreau–Yasuda magnetic bionanomaterial with gyrotactic micro-organisms, which is facilitated by radiative peristaltic transport. A compliant/elastic symmetric channel subject to partial slip constraints was chosen. The features of viscous dissipation and ohmic heating were incorporated into thermal transport. We use the Brownian and thermophoretic movement characteristics of the Buongiorno nanofluid model in this study. A set of nonlinear ordinary differential equations are created from the partial differential equations that control fluid flow. The governing system of differential equations is solved numerically via the shooting technique. The results of pertinent parameters are examined through velocity, temperature, motile micro-organisms, concentration, and heat transfer rate.

Keywords: bioconvection; gyrotactic micro-organism; peristalsis; Carreau–Yasuda fluid; thermal radiation; bionanomaterials



Citation: Nisar, Z.; Yasmin, H. Analysis of Motile Gyrotactic Micro-Organisms for the Bioconvection Peristaltic Flow of Carreau–Yasuda Bionanomaterials. *Coatings* **2023**, *13*, 314. <https://doi.org/10.3390/coatings13020314>

Academic Editor: Rafael Taboryski

Received: 30 December 2022

Revised: 24 January 2023

Accepted: 27 January 2023

Published: 31 January 2023



Copyright: © 2023 by the authors. Licensee MDPI, Basel, Switzerland. This article is an open access article distributed under the terms and conditions of the Creative Commons Attribution (CC BY) license (<https://creativecommons.org/licenses/by/4.0/>).

1. Introduction

Peristalsis is the term that refers to the movement of fluid caused by wave motion that is influenced by the sinusoidal wall of a channel or duct. The pharmaceutical, bio-engineering, facelifts, chemical, and paper industries all depend on the peristalsis process. Additional examples of peristaltic procedures in living organisms include the flow of sperm, ovum, urine, blood, food, and other bodily fluids. Peristaltic pumps are used in medical devices, such as fusion pumps, open-heart bypass pumps, and dialysis machines. With these issues in mind, Latham [1] conducted an earlier survey of peristaltic movement using both theoretical and empirical research methods. Since then, numerous researchers have looked into a variety of peristalsis-related topics in different flow circumstances. The small Reynolds number and large wavelength assumption with peristaltic pumping were later expanded by Shapiro et al. [2]. Mekheimer [3] has explored the features of the magnetic aspects for the peristalsis of couple stress fluids. Ali et al. [4] examined the thermal analysis for peristaltic in a curved channel. Wall characteristics for peristaltic transport of nanomaterial were studied by Mustafa et al. [5]. Hayat et al. [6] scrutinized the hall and convective aspects peristaltic flow of couple stress fluids. Sinnott et al. [7] inspected the particulate deferment in the small intestine, considering the activity of peristalsis. Yasmin et al. [8] studied the aspects of peristaltic transport with hall current and convective conditions. Nisar et al. [9] explored the characteristics of compliant walls and thermal radiation for

the peristaltic flow of nanoliquids. Yasmin et al. [10] examined the peristaltic flow of Johnson–Segalman fluids. Hina et al. [11] inquired about the peristaltic motion of non-Newtonian nanomaterials, considering the features of the electro-osmotic flow. Abbasi and Shehzad [12] developed a numerical solution for the peristaltic activity for ethylene-glycol and boron-nitride nanomaterials with a curved channel. Fluids with slip consequences have a wide spectrum of uses, including the buffing of artificial heart valves and inbuilt cavities. Slip aspects with peristaltic motion can be cited via [13–15].

Researchers and engineers became interested in assessing the flow of nanofluids for the advancement of the transport of heat. Nanofluids are used in a wide variety of industries and manufacturing fields, including microelectronics, geothermal panels, lubricating oil, nuclear reactors, biomedicine, pharmacological treatments, transportation, transformers, scintillating heat pipes, electronic devices, coolant in computers, lubricants in vehicles, nano-medicines, drug delivery, fermentation science, rubber sheet, factory production, heat exchanger design, and power generation. Due to its vast convenience, scientists and researchers have investigated nanomaterials as a result of their applications in various arenas of manufacturing and scientific processing. Choi and Eastman [16] coined the term “nanofluid” to characterize the use of conventional fluids with nano-sized diameters of less than 100 nm. Buongiorno [17] then gave a full investigation of nanofluids, in which he examined how Brownian movement and thermophoretic dispersion of nanoparticles lead to an increase in thermal conductivity. Tsai et al. [18] examined the effectiveness of gold nanoparticles in the thermal performance of heat pipes. Li et al. [19] examined the detailed analysis of nanofluids. Yan et al. [20] studied the speed of nanoparticles in nanomaterials via a zero-crossing laser speckle technique. Abbasi et al. [21] scrutinized the activity of peristalsis with copper-water nanofluids through permeable space. Akram et al. [22] reported the consequences of a magnetic field of a peristaltic pseudoplastic nanoliquid via a trapped channel. Bhatti and Abdelsalam [23] investigated the peristaltic activity of a hybrid nanofluid containing gold nanoparticles and tantalum while also considering its magnetic factors. Alsaedi et al. [24] reported the mixed convection and complaint wall characteristics for peristaltic flow for a nanofluid. Abbasi et al. [25] analyzed the electro-osmosis peristaltic flow of a hybrid nanofluid. Nisar et al. [26] reported the numerical investigation peristalsis of couple stress nanomaterials. Hussain et al. [27] examined the peristaltic flow of hybrid nanofluids. In their study, they analyzed how to enhance thermal conductivity with electro-osmosis-modulated peristaltic flow. Yasmin et al. [28] examined how hybrid nanofluids are useful in solar and thermal energy storage.

Bionanomaterials are nanoscale substances that are produced biologically. They display distinctive chemical, structural, optical, physical, electrical, biological, and mechanical features that set them apart from bulk matter due to their very compact size. Bionanomaterials, e.g., fungi, bacteria, plants, nucleic acids, peptides, etc., are promising materials made from numerous biological components. Due to their biological synthesis and biocompatibility, the use of bionanomaterials in the biomedical area has received considerable interest. Bionanomaterials, which are extraordinarily small, have unique qualities that give them potential in a variety of fields, including pharmacology, aeronautical engineering, material science, biosensors, and more. Moreover, a number of characterization techniques have been used to explore the characteristics of the synthesized bionanomaterials [29,30].

Numerous scientists and researchers have become fascinated by the study of non-Newtonian fluids in recent years. Studies on these fluids are encouraged by their significance in fields including industrial developments, plastic melting, pharmaceutical products, polymeric fluids, metabolic engineering, hazardous and nuclear facilities, industrial settings, and the food industry. Blood, perfumes, honey, diesel fuel, glue, cream, and many more substances are famous examples. Among these, the Carreau–Yasuda fluid framework [31] can explain the shear thinning and thickening features. Kayani et al. [32] examined the peristaltic flow of the Carreau–Yasuda model by adding nanoparticles. Khan et al. [33] examined the entropy generation analysis for a Carreau–Yasuda material with activation energy. Hayat et al. [34] explored the impact of modified Darcy’s expression for

peristaltic motion of Carreau–Yasuda nanoliquids via a chemical reaction. Iqbal and Abbasi [35] studied the MHD peristaltic activity of nanoliquid by analyzing a Carreau–Yasuda model via joule heating and variable thermal conductivity.

Bioconvection is the term used to describe organic macroscopic convective fluid motion. The bioconvection phenomenon is caused by the interaction of micro-organisms at various physical scales. The presence of directional movement of different types of micro-organisms is a prerequisite for various bioconvection systems. Gyrotactic micro-organisms are those that travel in water against the direction of gravity. The base fluid density is increased by these gyrotactic bacteria when they swim in a certain direction. Bioconvection is essential to bioengineering and bioimaging. According to the available data, several scientists have employed various bioconvection models to examine bioconvection movement mechanisms. Pedley et al. [36] studied the growth of bioconvection models in a uniform suspension of gyrotactic micro-organisms. Waqas et al. [37] examined a second-grade nanoliquid, including its gyrotactic micro-organisms. Rao et al. [38] explored the effects of gyrotactic micro-organisms for bioconvection in a convectational nanofluid. Hayat et al. [39] examined the slip and bioconvection aspects of the peristalsis of nanomaterials. Hussein et al. [40] discussed the bioconvective peristaltic flow of Jeffrey nanofluids. Akbar et al. [41] analyzed the peristaltic motion for motile gyrotactic micro-organisms of Eyring Powell nanoliquids. Avramenko et al. [42] reported the aspects of bioconvection instability of gyrotactic motile micro-organisms.

One of the areas of coating research that has had its fair share of successes and failures is compliant walls. The topic has fascinated, perturbed, and occasionally contented engineers and scientists for the past four decades as they search for ways to forgo the transition from laminar to turbulent flow, suppress flow-induced noise, reduce skin-friction drag in turbulent wall-bounded flows, and suppress vibrations [43,44]. The findings of Kramer [45] showed a compliant coating design based on dolphin epidermis, with reports of remarkable transition delay and drag reduction in hydrodynamic flows, which is what initially sparked interest in the topic. Regarding the dependability of the available analytical, numerical, and experimental data, there are several significant problems.

The present investigation looks at the impacts of bioconvective magnetohydrodynamic peristaltic Carreau–Yasuda bionanomaterials in a symmetric channel with gyrotactic micro-organisms. Compliant/stretchy channel walls are subjected to slip boundary conditions. A Carreau–Yasuda nanofluid is used in this study with integrated features of random motion and thermophoresis. The aspects of thermal radiation and ohmic heating are also considered. Numerical solutions for velocity, nanoparticle concentration, temperature, and motile micro-organism profiles were found. Finally, the key findings of the study are listed. This is a study that might be very useful in the field of biomedical and nanotechnology.

2. Problem Formulation

We consider two-dimensional peristaltic flow of a Carreau–Yasuda nanofluid. Here, we choose a symmetric channel of width $2d_1$. A Cartesian co-ordinate system (x, y) is used, such that the y -axis and x -axis are transverse and parallel to the channel walls. The motion of gyrotactic micro-organisms, which constitutes bioconvection, preserves the nanoparticles suspended in the nanofluid. The channel is subjected to a (B_0) constant magnetic field that is applied perpendicularly. The elastic walls are traversed by sinusoidal waves. The wall shapes are defined by [5].

$$y = \pm \eta(x, t) = \pm \left[d_1 + a \sin \frac{2\pi}{\lambda} (x - ct) \right], \quad (1)$$

where λ , c , and a denote wavelength, wave speed, and amplitude, respectively. The related expressions for Carreau–Yasuda fluid S are defined by [31,32].

$$S = \mu(\dot{\gamma}) A_1, \quad (2)$$

$$\mu(\dot{\gamma}) = \mu_\infty + (\mu_0 - \mu_\infty) \left[1 + (\Gamma \dot{\gamma})^a \right]^{\frac{n-1}{a}}, \tag{3}$$

$$\dot{\gamma} = \sqrt{2tr(D^2)}, D = \frac{1}{2}A_1 = \frac{1}{2}[(gradV) + (gradV)^T]. \tag{4}$$

From (3), μ_∞ and μ_0 represent the infinite and zero share rate viscosities. In the present study, we assumed that μ_∞ is zero. Further, Γ and a^* are the material variables. Additionally, n represents the power law index. The expression A_1 is the first Rivlin Ericksen tensor. The thermal transfer incorporates thermophoresis and Brownian motion. The expressions for the problem under these assumptions are as follows:

$$\frac{\partial u}{\partial x} + \frac{\partial v}{\partial y} = 0, \tag{5}$$

$$\begin{aligned} & \rho_f \left(\frac{\partial u}{\partial t} + u \frac{\partial u}{\partial x} + v \frac{\partial u}{\partial y} \right) \\ &= -\frac{\partial p}{\partial x} + \frac{\partial S_{xx}}{\partial x} + \frac{\partial S_{xy}}{\partial y} - \sigma B_0^2 u + g(1 - F_0)\rho_f \beta_T (T - T_0) \end{aligned} \tag{6}$$

$$- (\rho_p - \rho_f) g \beta_c (C - C_0) - (\rho_m - \rho_f) \gamma g (F - F_0),$$

$$\rho_f \left(\frac{\partial v}{\partial t} + u \frac{\partial v}{\partial x} + v \frac{\partial v}{\partial y} \right) = -\frac{\partial p}{\partial y} + \frac{\partial S_{yx}}{\partial x} + \frac{\partial S_{yy}}{\partial y} - \sigma B_0^2 v, \tag{7}$$

$$\left(\frac{\partial T}{\partial t} + u \frac{\partial T}{\partial x} + v \frac{\partial T}{\partial y} \right)$$

$$= \alpha \left(\frac{\partial^2 T}{\partial x^2} + \frac{\partial^2 T}{\partial y^2} \right) + \frac{1}{\rho_f c_f} \left\{ \frac{\partial u}{\partial x} S_{xx} + \frac{\partial v}{\partial y} S_{yy} + \left(\frac{\partial u}{\partial y} + \frac{\partial v}{\partial x} \right) S_{xy} \right\} \tag{8}$$

$$+ \tau \left[\left\{ \left(\frac{\partial T}{\partial y} \right)^2 + \left(\frac{\partial T}{\partial x} \right)^2 \right\} \frac{D_T}{T_m} + \left(\frac{\partial C}{\partial x} \frac{\partial T}{\partial x} + \frac{\partial C}{\partial y} \frac{\partial T}{\partial y} \right) D_B \right] + \frac{1}{\rho_f c_f} \sigma B_0^2 u^2 - \frac{\partial q_r}{\partial y},$$

$$\frac{\partial C}{\partial t} + u \frac{\partial C}{\partial x} + v \frac{\partial C}{\partial y} = \left(\frac{\partial^2 C}{\partial x^2} + \frac{\partial^2 C}{\partial y^2} \right) D_B + \frac{D_T}{T_m} \left(\frac{\partial^2 T}{\partial x^2} + \frac{\partial^2 T}{\partial y^2} \right), \tag{9}$$

$$\frac{\partial F}{\partial t} + u \frac{\partial F}{\partial x} + v \frac{\partial F}{\partial y} = -\frac{bW_c}{(C_1 - C_0)} \left(\frac{\partial}{\partial x} \left(F \frac{\partial C}{\partial x} \right) + \frac{\partial}{\partial y} \left(F \frac{\partial C}{\partial y} \right) \right) + \left(\frac{\partial^2 F}{\partial x^2} + \frac{\partial^2 F}{\partial y^2} \right) D_N. \tag{10}$$

The subjected boundary conditions are

$$u \pm \beta_1 S_{xy} = 0 \text{ at } y = \pm \eta, \tag{11}$$

$$\begin{aligned} \left(-\tau_1 \frac{\partial^3}{\partial x^3} + m_1 \frac{\partial^3}{\partial x \partial t^2} + d \frac{\partial^2}{\partial t \partial x} \right) \eta &= \frac{\partial S_{xx}}{\partial x} + \frac{\partial S_{xy}}{\partial y} - \rho_f \left(\frac{\partial u}{\partial t} + u \frac{\partial u}{\partial x} + v \frac{\partial u}{\partial y} \right) - \\ & \sigma B_0^2 u + g(1 - F_0)\rho_f \beta_T (T - T_0) - (\rho_p - \rho_f) g \beta_c (C - C_0) - \\ & - (\rho_p - \rho_f) \gamma g (F - F_0) \text{ at } y = \pm \eta, \end{aligned} \tag{12}$$

$$T \pm \beta_2 \frac{\partial T}{\partial y} = \left\{ \frac{T_1}{T_0} \right\}, C \pm \beta_3 \frac{\partial C}{\partial y} = \left\{ \frac{C_1}{C_0} \right\}, F = \left\{ \frac{F_1}{F_0} \right\} \text{ at } y = \pm \eta. \tag{13}$$

In the above equations, (v, u) designate the components of velocity in the (y, x) plane, (ρ_p) is the density of the nanoparticles, (ρ_f) is the nanofluid density, (ρ_m) is the motile micro-organisms density, (g) is gravity, (D_N) is the micro-organisms diffusion coefficient, (v) is for kinematic viscosity, (σ) is for electric conductions, (p) is for pressure and (α) is for thermal diffusivity, and (d) is for viscous damping coefficient. Further, (D_T) describes the thermophoretic diffusion and Brownian movement coefficient, (D_B) , $\tau (= (\rho_c)_p / (\rho_c)_f)$, for the ratio of the liquid’s heat capacity to the material’s effective heat capacity, (γ) is the average volume of the micro-organisms, (b) is the chemotaxis constant, (τ_1) is the tension of the elastic, (W_c) is the maximum cell-swimming speed, (m_1) is the area per unit mass,

(T_m) is the mean temperature, C_1, C_0 and T_1, T_0 are the concentration and temperature at the top and lower walls, respectively. Further, (F_1, F_0) is the fraction volume at the upper and lower walls. The radiant heat flow satisfies the Rossland approach:

$$q_r = -\frac{4\bar{\sigma}}{3k} \frac{\partial T^4}{\partial y}, \tag{14}$$

where ($\bar{\sigma}, \bar{k}$) are the constant of the Stefan–Boltzman coefficients and mean absorption, respectively. The expanded form of T^4 can be written as

$$T^4 = 4T_0^3 T - 3T_0^4, \tag{15}$$

thus, we have

$$q_r = -\frac{16\bar{\sigma}T_0^3}{3k} \frac{\partial T}{\partial y}. \tag{16}$$

When considering stream function $u = \psi_y, v = -\delta(\psi_x)$, and using the nondimensional variables:

$$\begin{aligned} u^* &= \frac{u}{c}, v^* = \frac{v}{c}, \chi^* = \frac{x}{\lambda}, y^* = \frac{y}{d_1}, t^* = \frac{ct}{\lambda}, \eta^* = \frac{\eta}{d_1}, p^* = \frac{d_1^2 p}{c\lambda\mu_0}, \\ \theta &= \frac{T-T_0}{T_1-T_0}, \phi = \frac{C-C_0}{C_1-C_0}, \beta_1^* = \frac{\beta_1\mu_0}{d_1}, \beta_i^* = \frac{\beta_i}{d_1} (i = 2, 3), \\ S_{ij}^* &= \frac{d_1 S_{ij}}{c\mu_0}, \chi = \frac{F-F_0}{(F_1-F_0)}, \zeta = \frac{F_0}{(F_1-F_0)}. \end{aligned} \tag{17}$$

in Equations (5)–(13). After omitting the asterisk, we can write

$$\begin{aligned} \frac{\partial^2}{\partial y^2} \left(1 + \frac{We^{a^*}(n-1)(1-\beta)}{a^*} \left(\frac{\partial^2 \psi}{\partial y^2} \right)^{a^*} \right) \frac{\partial^2 \psi}{\partial y^2} - M^2 \frac{\partial^2 \psi}{\partial y^2} + Gr \frac{\partial \theta}{\partial y} - Gc \frac{\partial \phi}{\partial y} \\ - Gf \frac{\partial \chi}{\partial y} = 0, \end{aligned} \tag{18}$$

$$(1 + PrRn) \frac{\partial^2 \theta}{\partial y^2} + NbPr \frac{\partial \theta}{\partial y} \frac{\partial \phi}{\partial y} + NtPr \left(\frac{\partial \theta}{\partial y} \right)^2 + BrM^2 \left(\frac{\partial \psi}{\partial y} \right)^2 + BrS_{xy} \frac{\partial^2 \psi}{\partial y^2} = 0, \tag{19}$$

$$Nt \frac{\partial^2 \theta}{\partial y^2} + Nb \frac{\partial^2 \phi}{\partial y^2} = 0, \tag{20}$$

$$\frac{\partial^2 \chi}{\partial y^2} - Pe \frac{\partial \chi}{\partial y} \frac{\partial \phi}{\partial y} - Pe\zeta \frac{\partial^2 \phi}{\partial y^2} - Pe\chi \frac{\partial^2 \phi}{\partial y^2} = 0. \tag{21}$$

The boundary conditions become

$$\frac{\partial \psi}{\partial y} \pm \beta_1 \left[\frac{\partial^2 \psi}{\partial y^2} + \frac{(1-\beta)(n-1)We^{a^*}}{a^*} \left(\frac{\partial^2 \psi}{\partial y^2} \right)^{a^*+1} \right] = 0 \text{ at } y = \pm \eta, \tag{22}$$

$$\begin{aligned} & \left[E_1 \frac{\partial^3}{\partial x^3} + E_2 \frac{\partial^3}{\partial x \partial t^2} + E_3 \frac{\partial^2}{\partial x \partial t} \right] \eta \\ &= \frac{\partial^3 \psi}{\partial y^3} + \frac{\partial}{\partial y} \left[\frac{\partial^2 \psi}{\partial y^2} + \frac{(1-\beta)(n-1)We^{a^*}}{a^*} \left(\frac{\partial^2 \psi}{\partial y^2} \right)^{a^*+1} \right] \\ & - M^2 \frac{\partial \psi}{\partial y} + Gr\theta - Gc\phi - Gf\chi \text{ at } y = \pm \eta, \end{aligned} \tag{23}$$

$$\theta \pm \beta_2 \frac{\partial \theta}{\partial y} = \left\{ \begin{matrix} 1 \\ 0 \end{matrix} \right\}, \phi \pm \beta_3 \frac{\partial \phi}{\partial y} = \left\{ \begin{matrix} 1 \\ 0 \end{matrix} \right\}, \chi = \left\{ \begin{matrix} 1 \\ 0 \end{matrix} \right\} \text{ at } y = \pm \eta. \tag{24}$$

The continuity in Equation (5) is automatically satisfied. In the above expression, we witnessed that the small Reynolds number and large wavelength suppositions [2] are in-

voked. Here, $\varepsilon, \delta, Ec, Re, Pr, M, Sc, Br, Nb, Nt, We, Rn, (E_1, E_2, E_3), Gc, Pe, Gf, Gr$, and β are ratio of amplitude, wave number, Eckert number, Reynolds and Prandtl numbers, Hartman number, Schmidt number, Brinkman number, Brownian motion variable, thermophoresis parameter, Weissenberg number, radiation parameter, elasticity parameters, concentration Grashof variable, Bioconvection Peclet number, Bioconvection Grashof number, thermal Grashof number, and viscosity ratio parameter, respectively. These are defined by

$$\begin{aligned} \varepsilon &= \frac{a}{d_1}, \delta = \frac{d_1}{\lambda}, Ec = \frac{c^2}{c_f(T_1 - T_0)}, Re = \frac{\rho c d_1}{\mu_0}, Pr = \frac{\nu}{\alpha}, M = \sqrt{\frac{\sigma}{\mu_0}} B_0 d_1, \\ Sc &= \frac{\nu}{D_B}, Br = Pr Ec, Nb = \frac{D_B \tau (C_1 - C_0)}{\nu}, Nt = \frac{D_T \tau (T_1 - T_0)}{T_m \nu}, We = \frac{\Gamma c}{d_1}, \\ Rn &= \frac{16 \bar{\sigma} T_0^3}{3 k k^*}, E_1 = -\frac{d_1^3 \tau}{\lambda^3 \mu_0 c}, E_2 = \frac{c m_1 d_1^3}{\lambda^3 \mu_0}, E_3 = \frac{d_1^3 d}{\lambda^2 \mu_0}, \\ Gc &= \frac{g \beta c (\rho_p - \rho_f) d_1^2 (C_1 - C_0)}{\mu_0 c}, Pe = \frac{b W_c}{D_N}, Gf = \frac{(\rho_m - \rho_f) g \gamma (F_1 - F_0) d_1^2}{\mu_0 c}, \\ Gr &= \frac{g \beta \tau (1 - F_0) \rho_f (T_1 - T_0) d_1^2}{\mu_0 c}, \beta = \frac{\mu_\infty}{\mu_0}. \end{aligned} \quad (25)$$

3. Numerical Method

The system constituting Equations (18)–(21) with the associated boundary conditions (22)–(24) are solved numerically via the shooting method by the program NDSolve using the fourth-order Runge–Kutta algorithm with the help of Mathematica. This approach helps with tiny step size errors and small errors and has strong internal consistency for boundary value problems.

4. Results and Discussion

The results for velocity, temperature, and the profiles of the motile micro-organisms were examined graphically. Further, the nanoparticle concentrations and rates of heat transfer were scrutinized by tabling the results.

4.1. Velocity

The consequences of the relevant parameters for velocity are presented in Figures 1–8. The effect of the velocity slip parameter, β_1 , is depicted in Figure 1. It was noticed that the velocity of the fluid arises via the velocity slip parameter β_1 . Figure 2 demonstrates the aspects of the Grashof number, Gr , against velocity. An enhancement in temperature is observed against the Grashof number Gr . The sketch of the bioconvection Rayleigh variable, Gf , is illustrated in Figure 3. As we can see, the velocity of the fluid declines with a larger Gf . The features of the buoyancy ratio variable, Gc , on the velocity profile are shown in Figure 4. The graph represents how the Gc boosts fluid velocity. The impacts of the Hartman number, M , on the velocity are revealed in Figure 5. This graph makes it clear that the liquid's velocity is decreasing. The implications of the bioconvection Peclet number Pe , on the velocity profile can be seen in Figure 6. The observed outcomes show that a rise in Pe increases the velocity. The impact of the Weissenberg number, We , is portrayed against velocity (see Figure 7). In this figure, we can see that the velocity of the liquid increases. The wall parameters E_1, E_2 , and E_3 are exhibited in Figure 8. It was detected that velocity is an increasing function of E_1 and E_2 , and it decreases for E_3 in view of the damping effect.

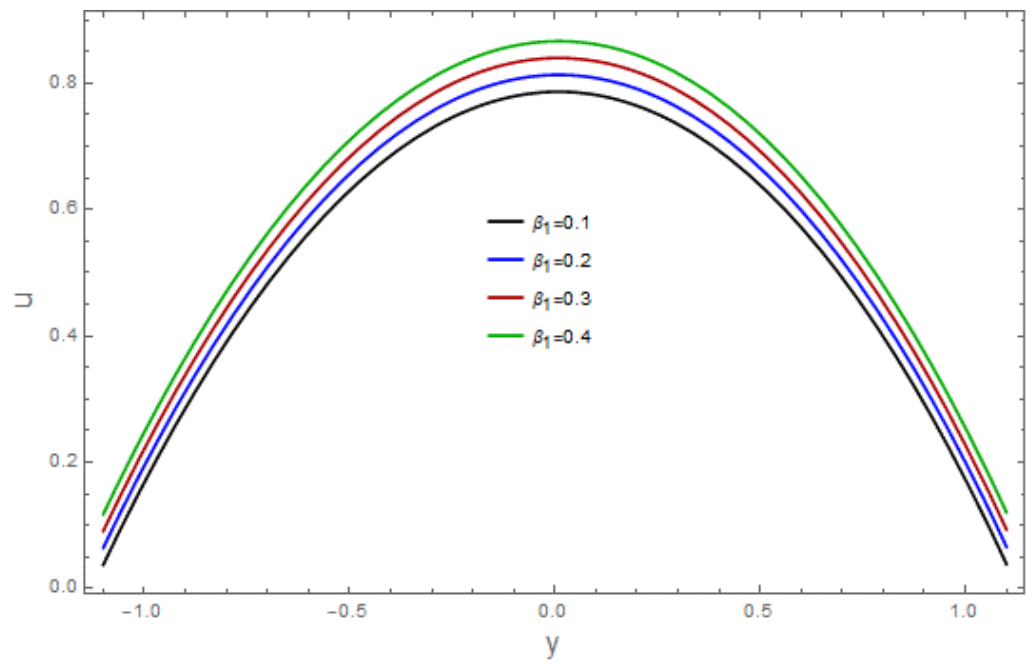


Figure 1. Effect of β_1 on u .

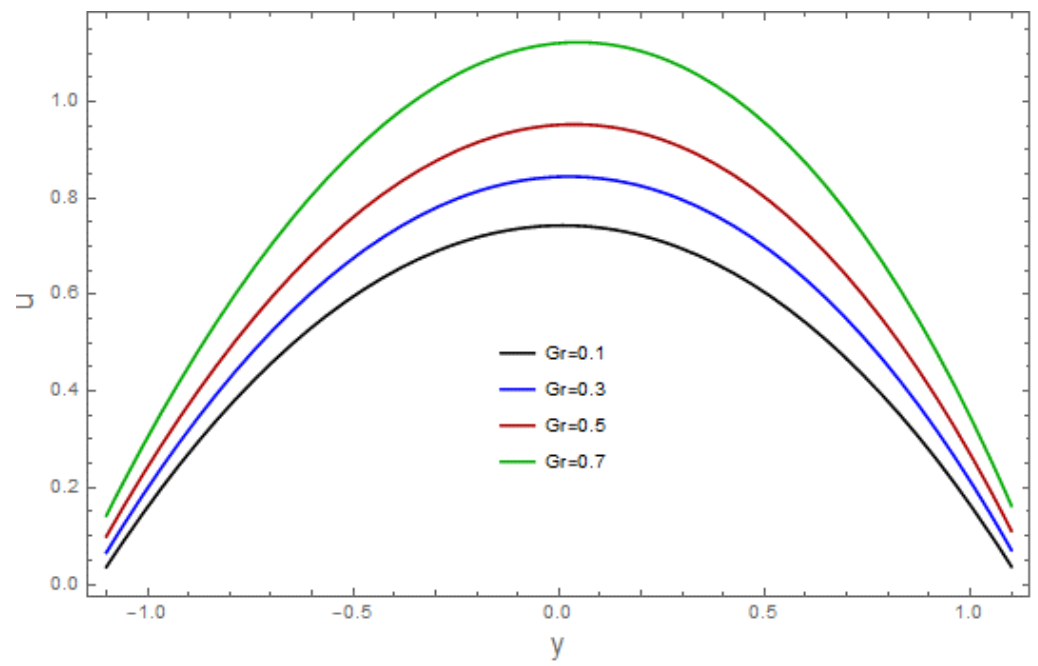


Figure 2. Effect of Gr on u .

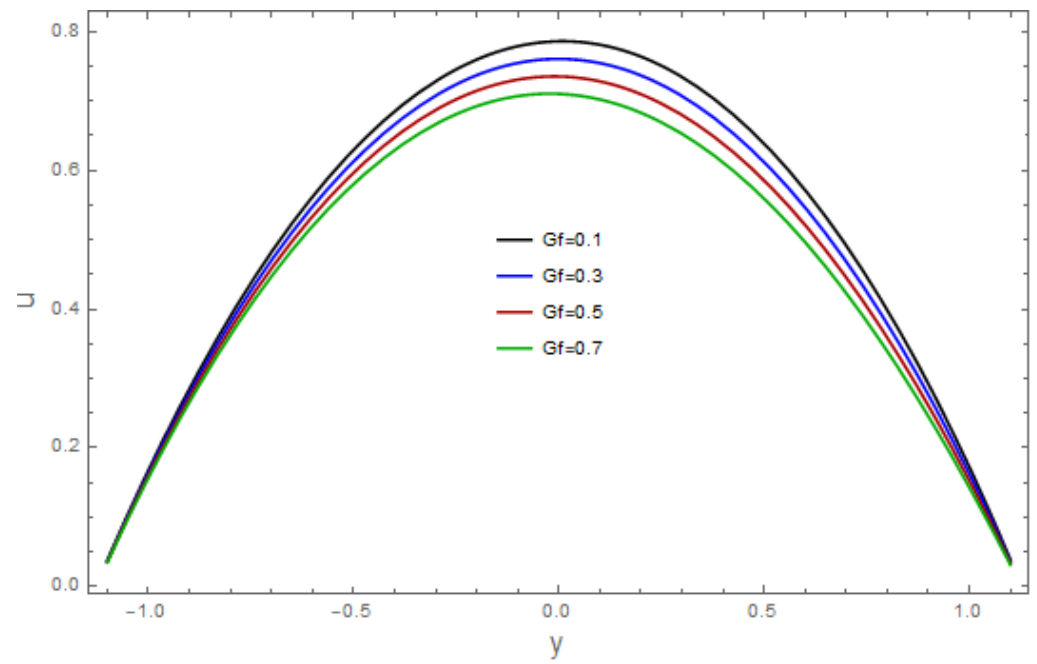


Figure 3. Effect of Gf on u .

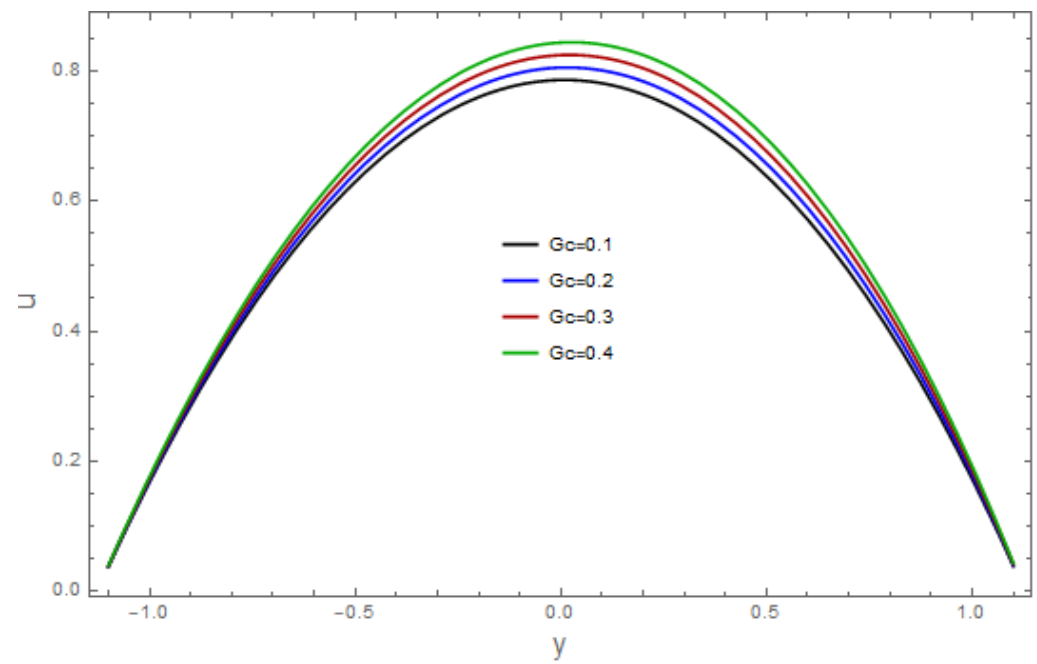


Figure 4. Effect of Gc on u .

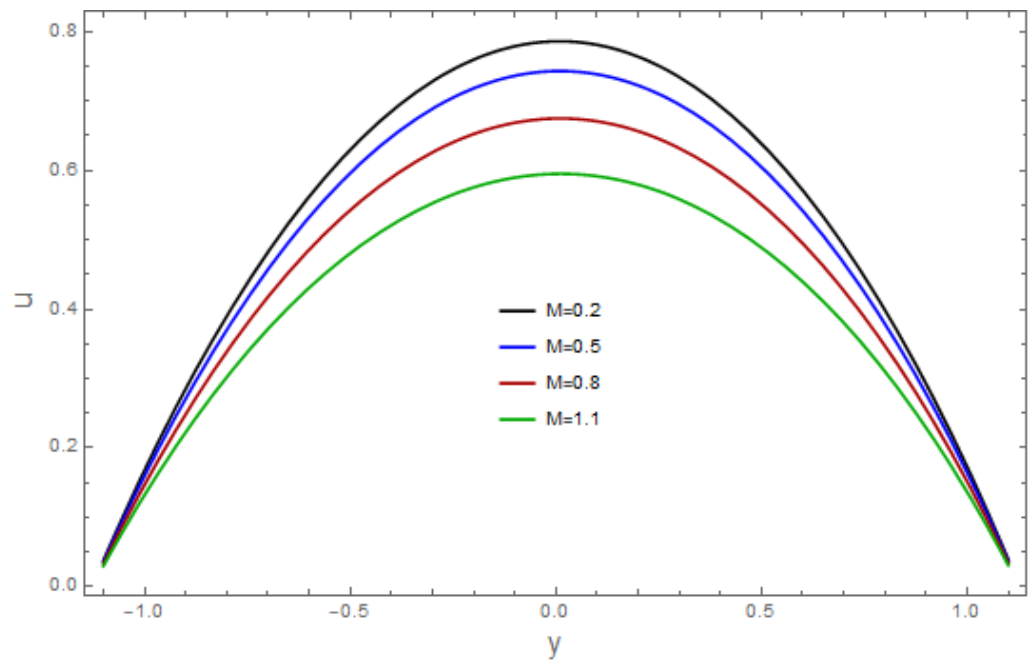


Figure 5. Effect of M on u .

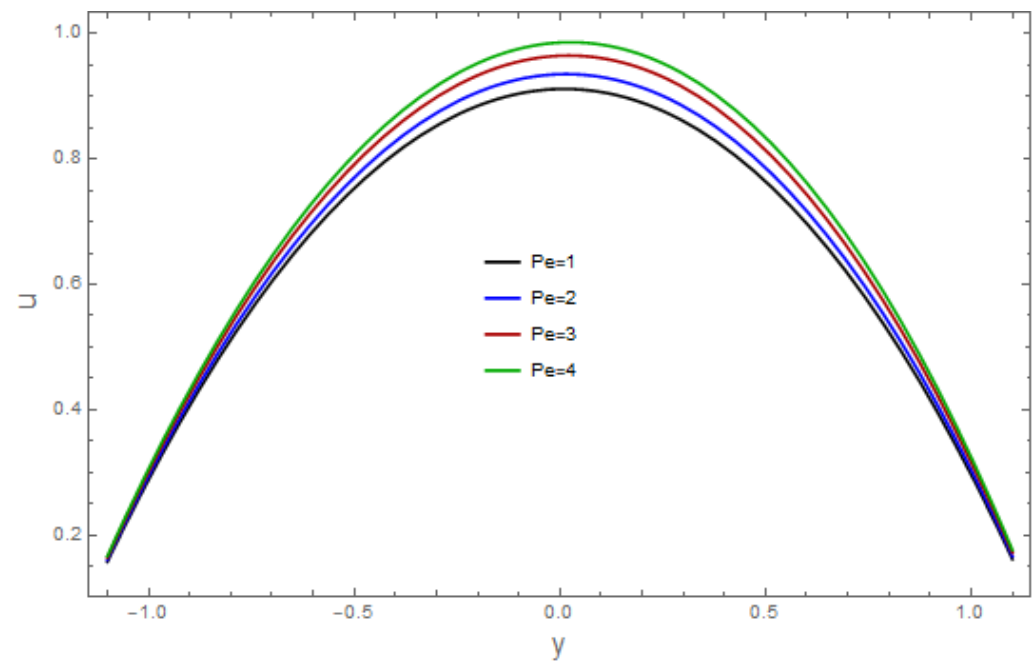


Figure 6. Effect of Pe on u .

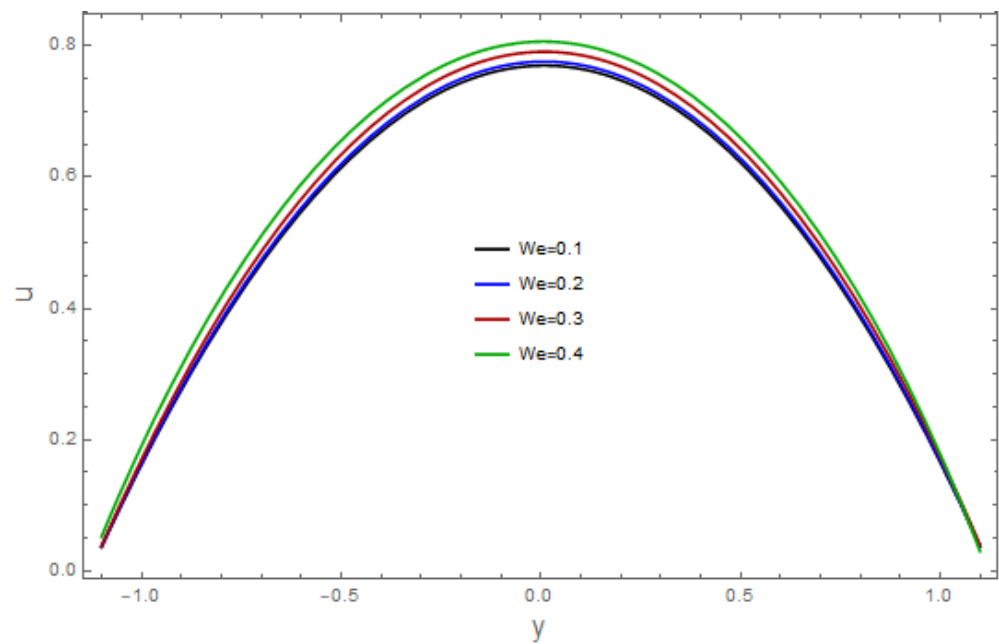


Figure 7. Effect of We on u .

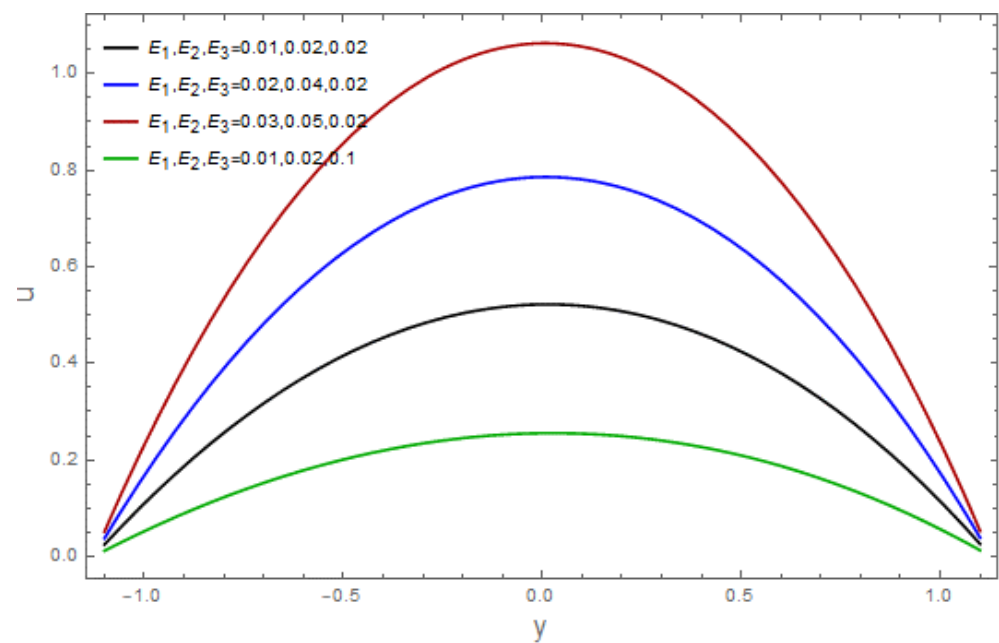


Figure 8. Effects of E_1 , E_2 and E_3 on u .

4.2. Temperature

The influence of various pertinent parameters on temperature θ is captured through Figures 9–17. Figure 9 represents the outcomes of the bioconvection Rayleigh parameter, Gf , with temperature. The temperature of the fluid declines as the bioconvection Rayleigh variable, Gf , increases. The influence of the Grashof number, Gr , on temperature is displayed in Figure 10. As we can see, increasing the values of Gr causes the material's temperature to increase. Figure 11 depicts the thermal field against the Brownian movement variables Nb . With increasing Brownian diffusion, Nb , the average kinetic energy of the fluid increases. As a result, the temperature acclivities. Figure 12 depicts the effect of the thermal radiation parameter Rn on the temperature. This graph demonstrates that the temperature declines when the radiation variable, Rn , increases. Figure 13 portrays the

impressions of the Brinkman variable, Br , on the temperature. As a high Brinkman variable, Br , intensifies, the outcomes of the viscous dissipation results in temperature acclivities. The impact of the thermal slip parameter, β_2 , is shown via Figure 14. By enhancing the values of the thermal slip parameter, β_2 , we can see that temperature increases. The effects of the buoyancy ratio variable, G_c , are displayed in Figure 15. An increasing trend is noticed for temperature vs. the buoyancy ratio variable G_c . The thermal field vs. the Weissenberg number, We , is shown in Figure 16. The temperature decreases as the mass Weissenberg number, We , increases. The consequences of the wall parameters E_1 , E_2 , and E_3 are presented in Figure 17 for temperature. It is shown that temperature is an increasing function of E_1 and E_2 , and it decreases with E_3 in view of the damping outcome.

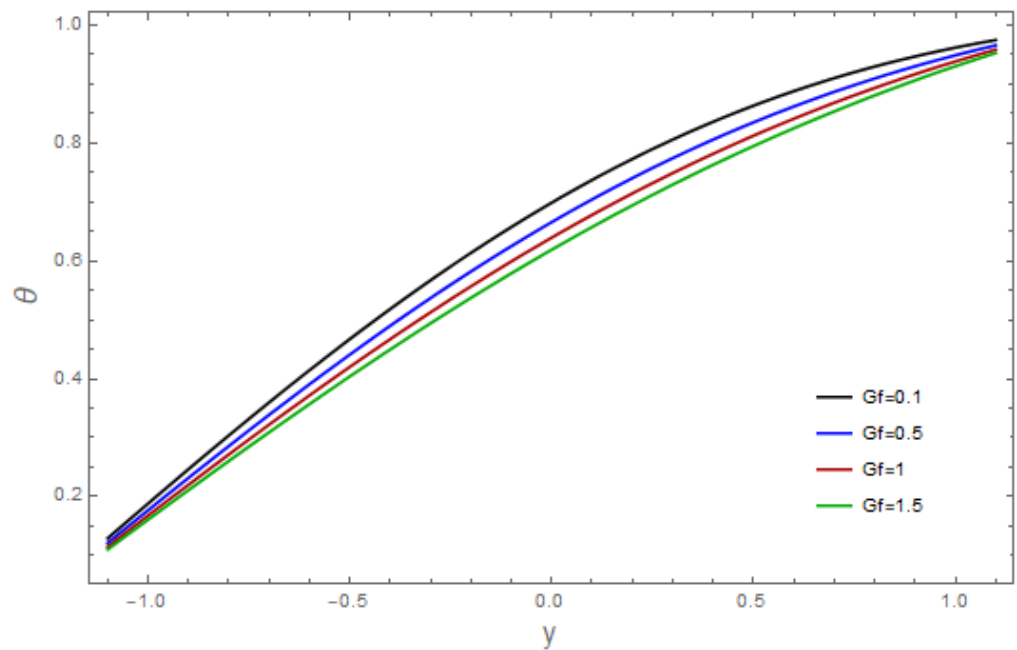


Figure 9. Effect of G_f on θ .

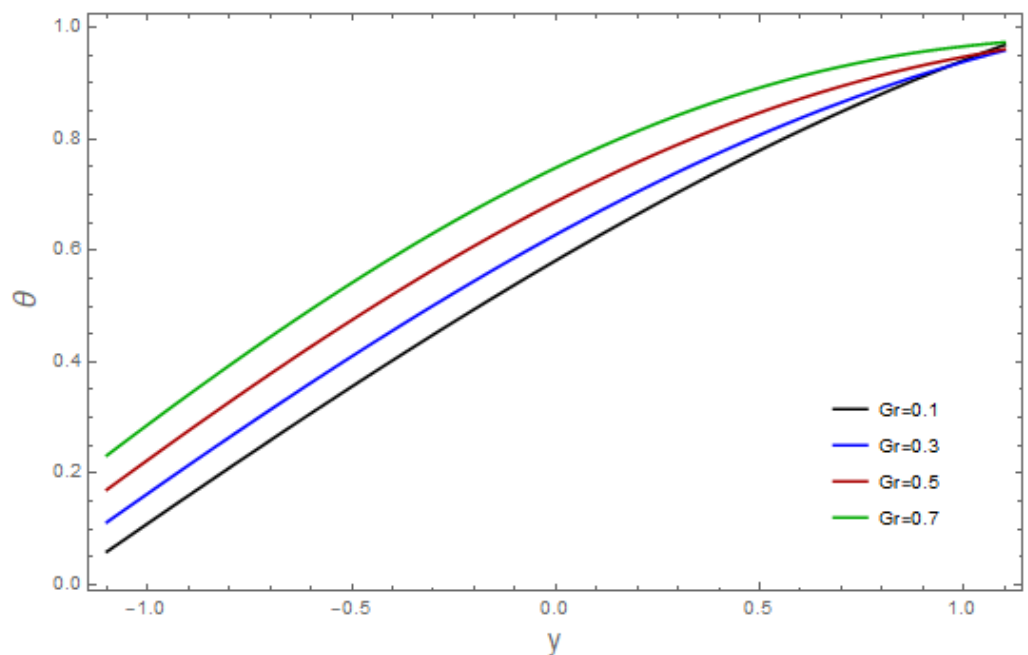


Figure 10. Effect of Gr on θ .

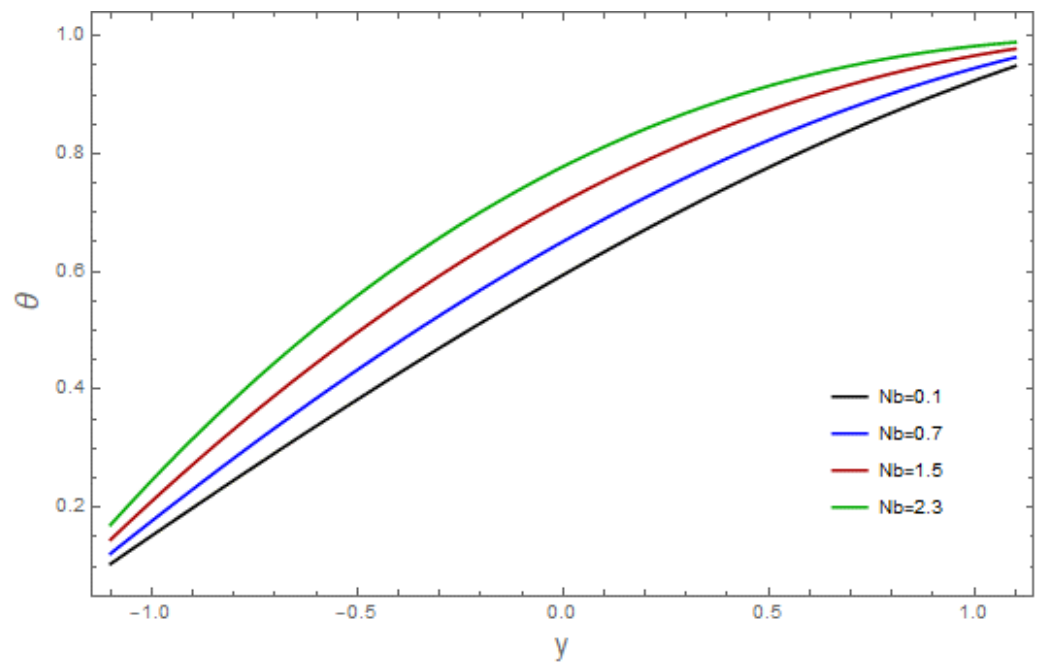


Figure 11. Effect of Nb on θ .

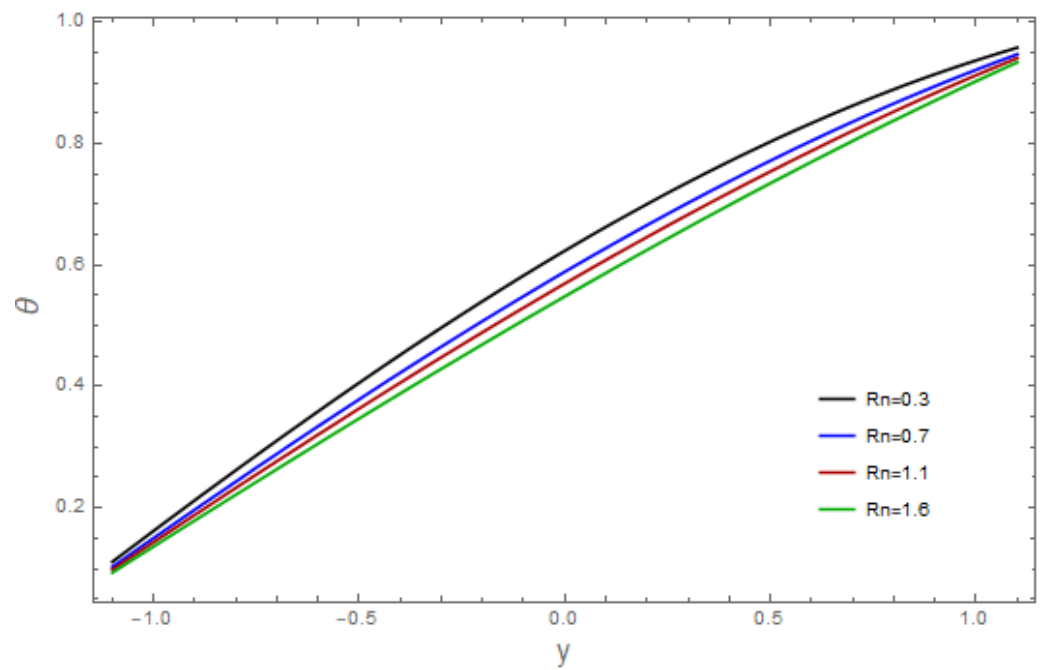


Figure 12. Effect of Rn on θ .

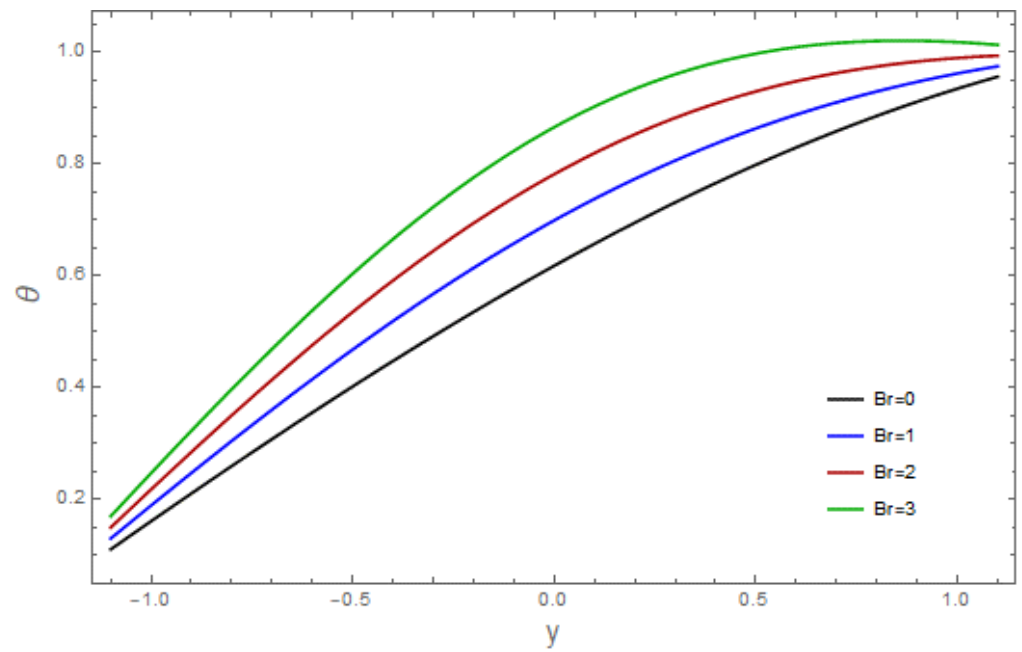


Figure 13. Effect of Br on θ .

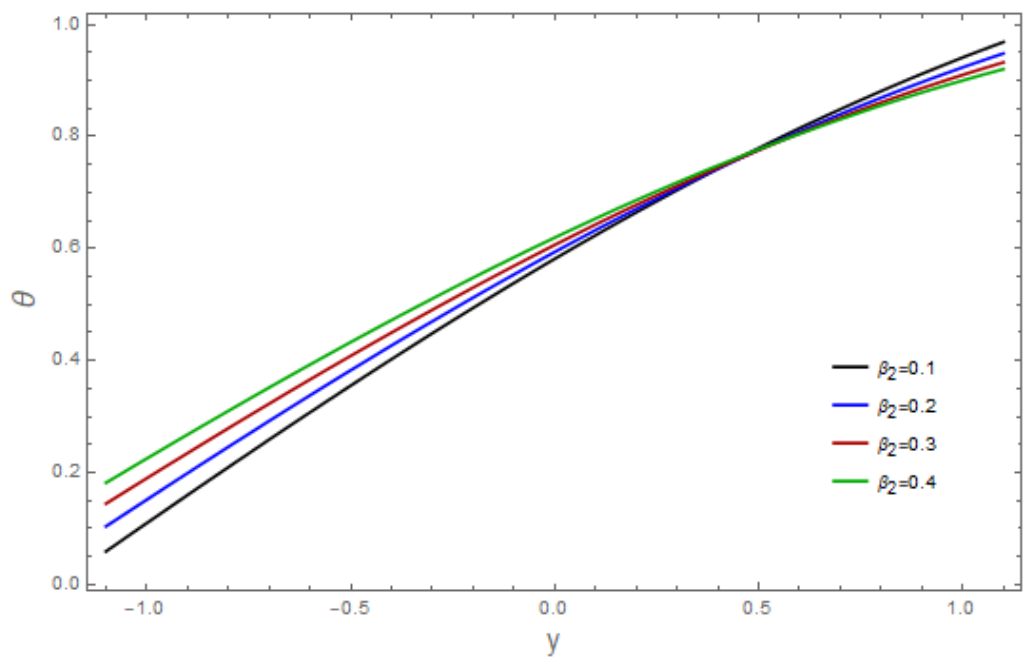


Figure 14. Effect of β_2 on θ .

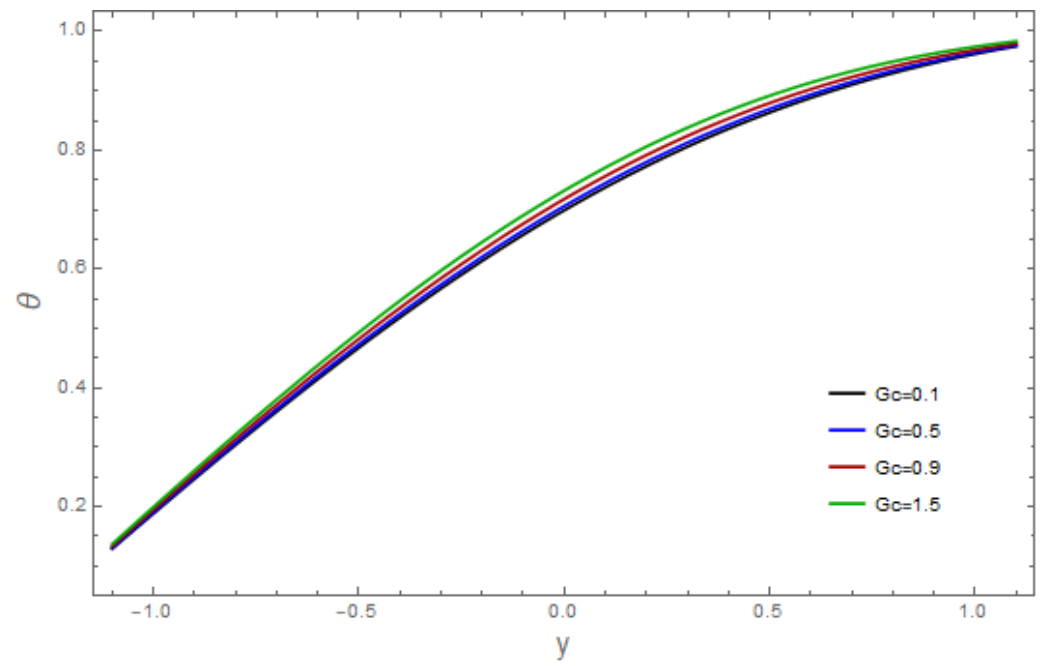


Figure 15. Effect of Gc on θ .

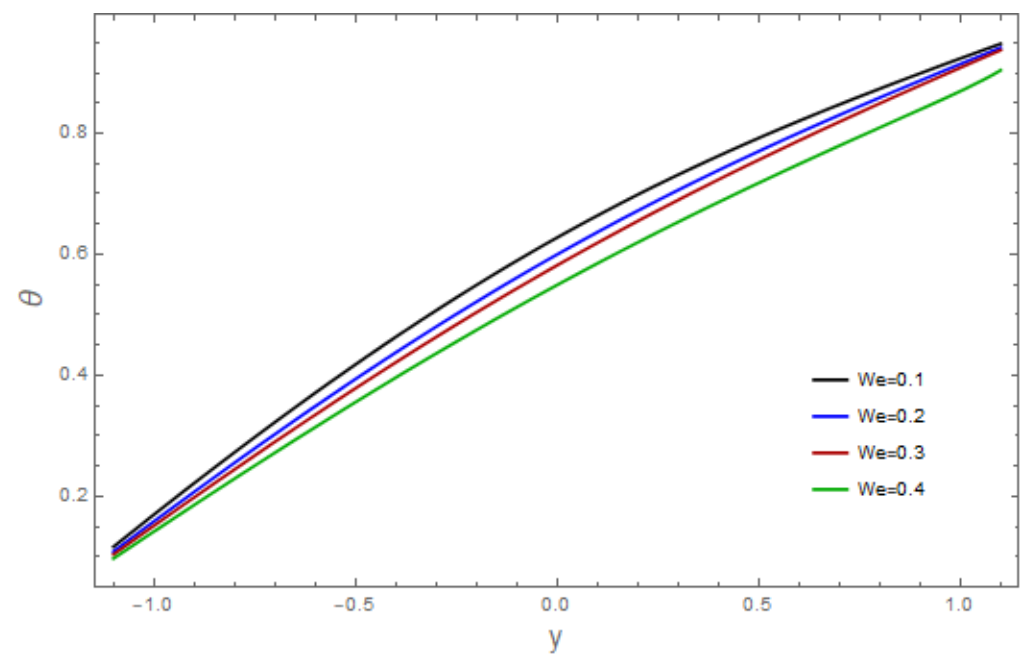


Figure 16. Effect of We on θ .

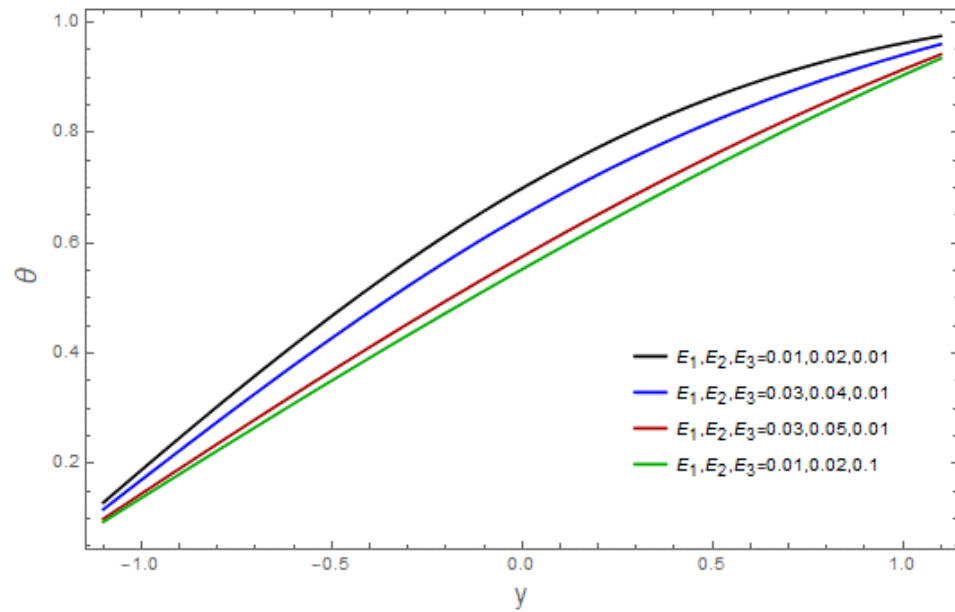


Figure 17. Effects of E_1, E_2 and E_3 on θ .

4.3. Profiles of Motile Micro-Organisms

Figures 18–22 show the influence of the measured variables on the profiles of the motile micro-organisms χ . The influence of the bioconvection Peclet number, Pe , is presented in Figure 18 against the motile micro-organisms profiles. It is shown that the motile micro-organisms profiles decline with an increasing bioconvection Peclet number Pe . Figure 19 presents the results for ζ . The motile micro-organisms profile increases with increases in ζ . The impact of the thermophoresis variable, Nt , on the profile of the motile micro-organisms is displayed in Figure 20. An increment in the thermophoresis variable, Nt , decreases the profile of the motile micro-organisms. The bioconvection Rayleigh variable, Gf , is exhibited in Figure 21. From this figure, it can be seen that the motile micro-organisms profile, χ , decreases for the bioconvection Rayleigh variable Gf . Figure 22 shows the Weissenberg number We . As can be seen in this figure, the micro-organisms profile, χ , of the fluid declines via the Weissenberg number We .

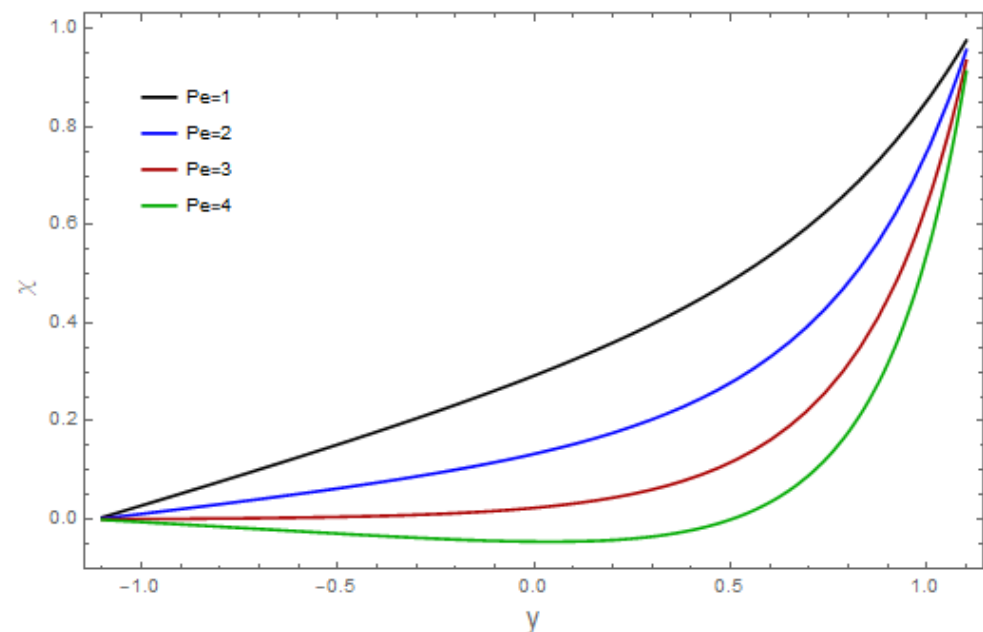


Figure 18. Effect of Pe on χ .

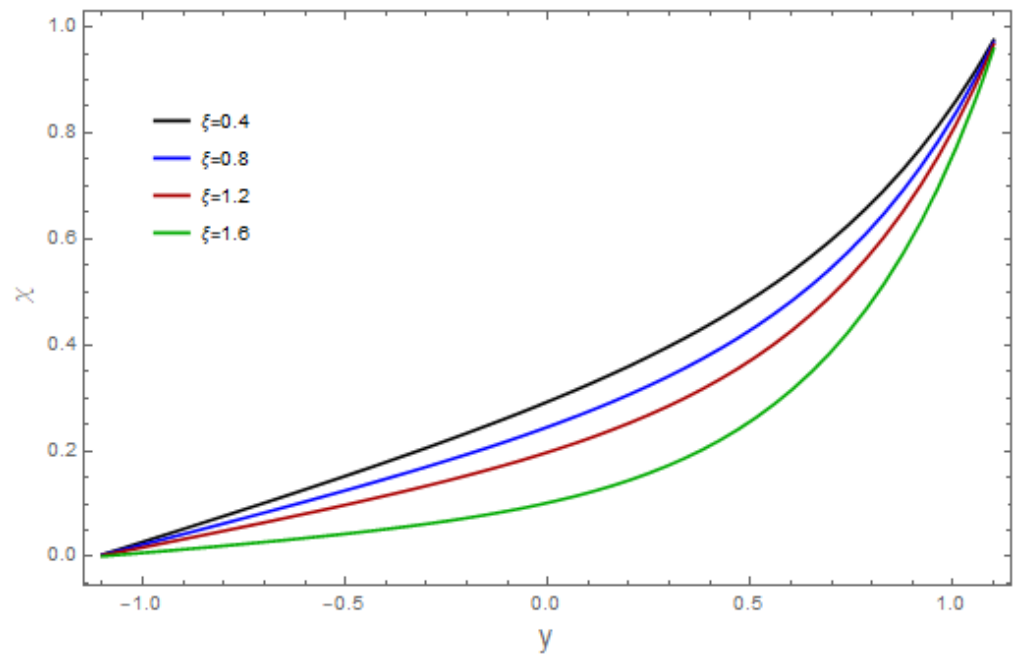


Figure 19. Effect of ζ on χ .

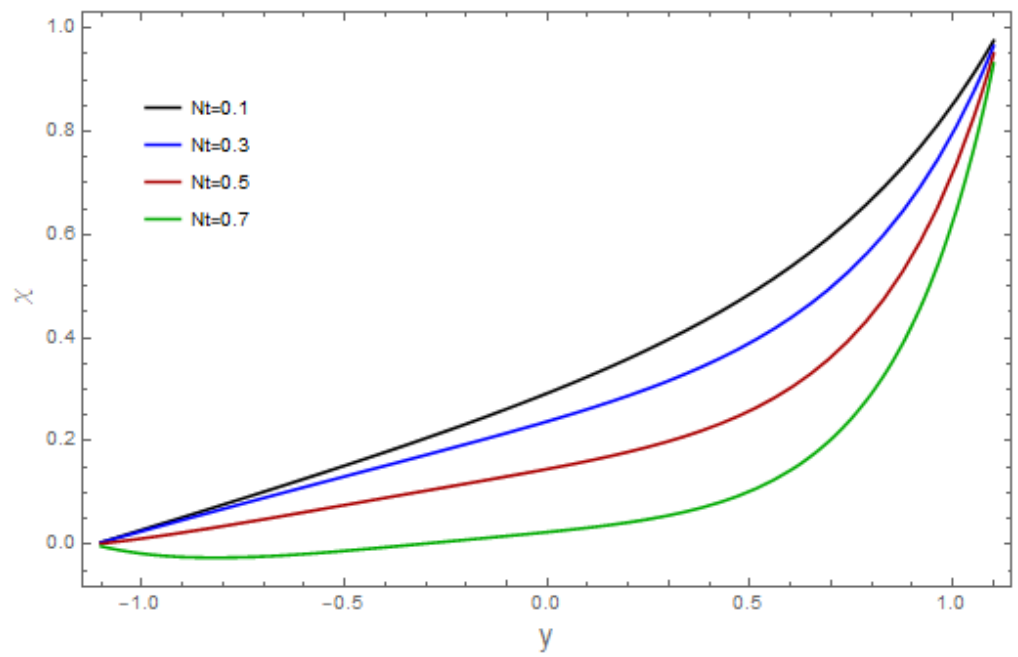


Figure 20. Effect of Nt on χ .

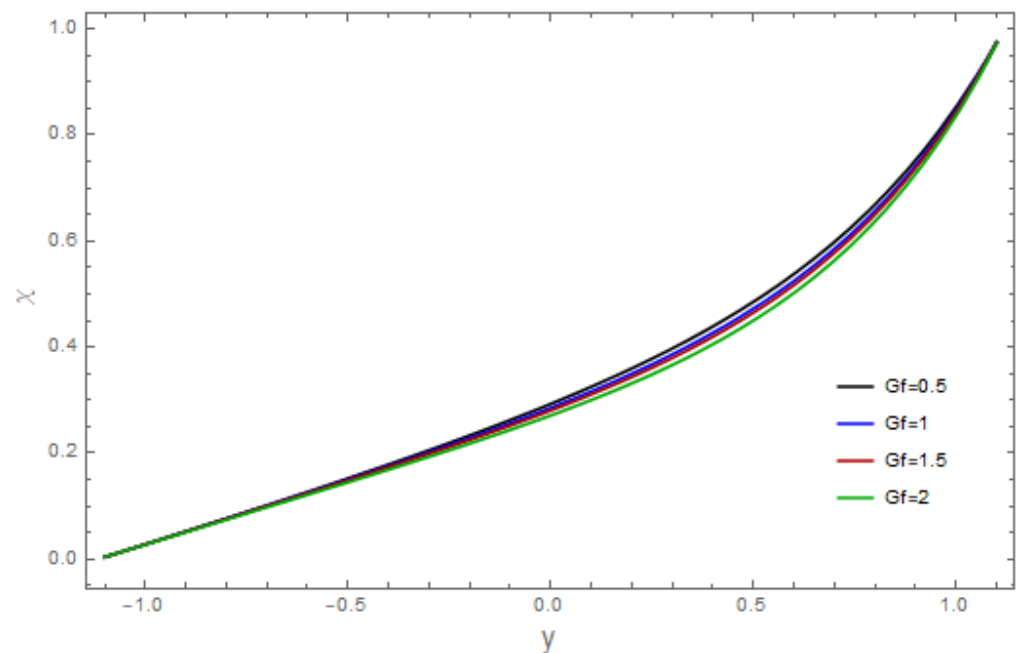


Figure 21. Effect of Gf on χ .

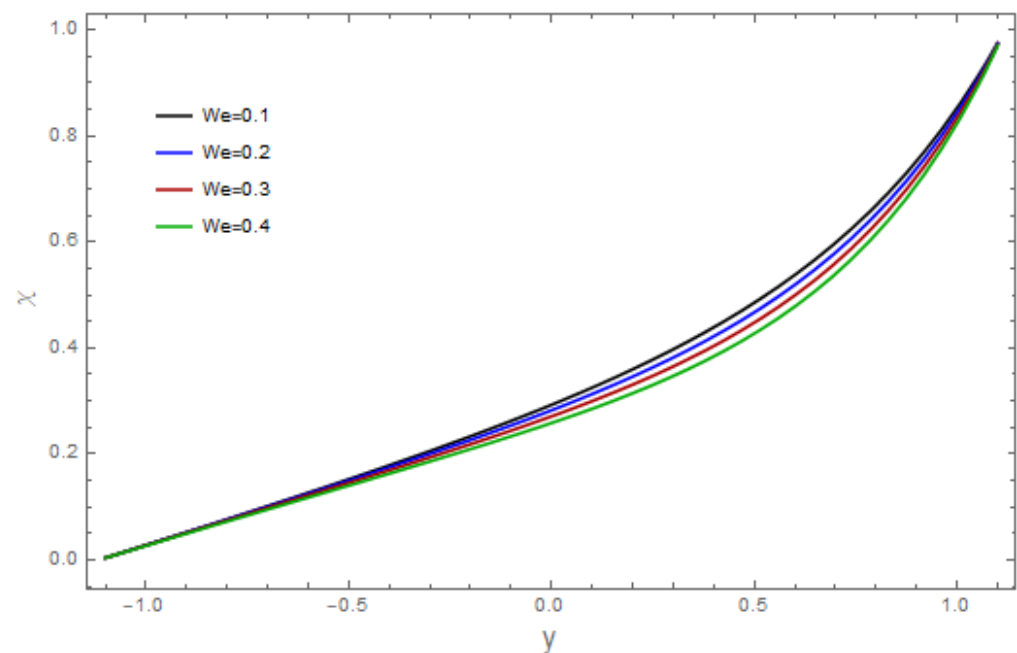


Figure 22. Effect of We on χ .

4.4. Concentration

The impacts of different pertinent variables, like ζ , β_3 , Gf , Gc , Pe , Nb , and Nt , on concentration $\phi(0)$ are displayed in Table 1. The concentration field decreases in the presence of ζ . By enhancing the values of the mass slip variable, β_3 , the concentration decreases. It is observed that the concentration field is an increasing function of the Rayleigh variable Gf . The concentration of the nanofluid decreases as the value of the buoyancy ratio parameter, Gc , increases. In the presence of the bioconvection Peclet number, Pe , the concentration field decreases. The concentration of the nanofluid has the opposite behavior for the thermophoresis, Nt , and Brownian movement, Nb , variables.

Table 1. Influences of distinct physical variables on $\phi(0)$.

ζ	β_3	Gf	Gc	Pe	Nb	Nt	$\phi(0)$
0.5	0.1	0.3	0.2	2	0.1	0.1	0.18773
1							0.18648
0.5	0.2						0.16171
	0.3						0.13874
	0.1	0.5					0.18979
		0.9					0.19382
		0.3	0.5				0.18171
			0.9				0.17599
			0.2	3			0.18593
				4			0.18468
				2	0.4		0.27067
					0.7		0.28265
					0.1	0.2	0.06122
						0.3	0.03627

4.5. Heat Transfer Rate

The influence of the sundry variables on the rate of heat transfer, $-\theta'(\eta)$ is examined in Table 2. The results of the bioconvection Rayleigh parameter, Gf , are displayed in Table 2. It can be noticed that the rate of heat transfer declines. The rate of heat transfer declines via the Weissenberg number We . Increasing the Brownian movement, Nb , variable enhances the rate of heat transfer. An increasing trend is noticed for the Grashof number Gr . It is shown that the rate of heat transfer increases via the bioconvection Peclet parameter Pe . The heat transfer rate declines via the thermal radiation variable Rn and viscosity ratio parameter β .

Table 2. Influences of distinct physical variables on $-\theta'(\eta)$.

Gf	We	Nb	Gr	Pe	Rn	β	$-\theta'(\eta)$
0.5	0.3	4	0.5	1	1.5	0.1	0.0367749
0.7							0.0279817
0.5	0.4						0.0342317
	0.5						0.0127678
	0.3	5					0.048036
		6					0.0553885
		4	0.7				0.0651841
			0.9				0.0974947
			0.5	1.5			0.0435089
				2			0.0492939
				1	1		0.0836686
					1.8		0.0112577
					1.5	0.2	0.0367803
						0.5	0.0365506

4.6. Trapping

Plots for the trappings are drawn in Figures 23 and 24. Figure 23a,b is plotted for the Weissenberg number We . From this Figure, we noticed that the size of the bolous increases. Figure 24a,b is plotted to see the impact of the Hartman number; as we can see, an increment in the Hartman number increases the size of the bolous.

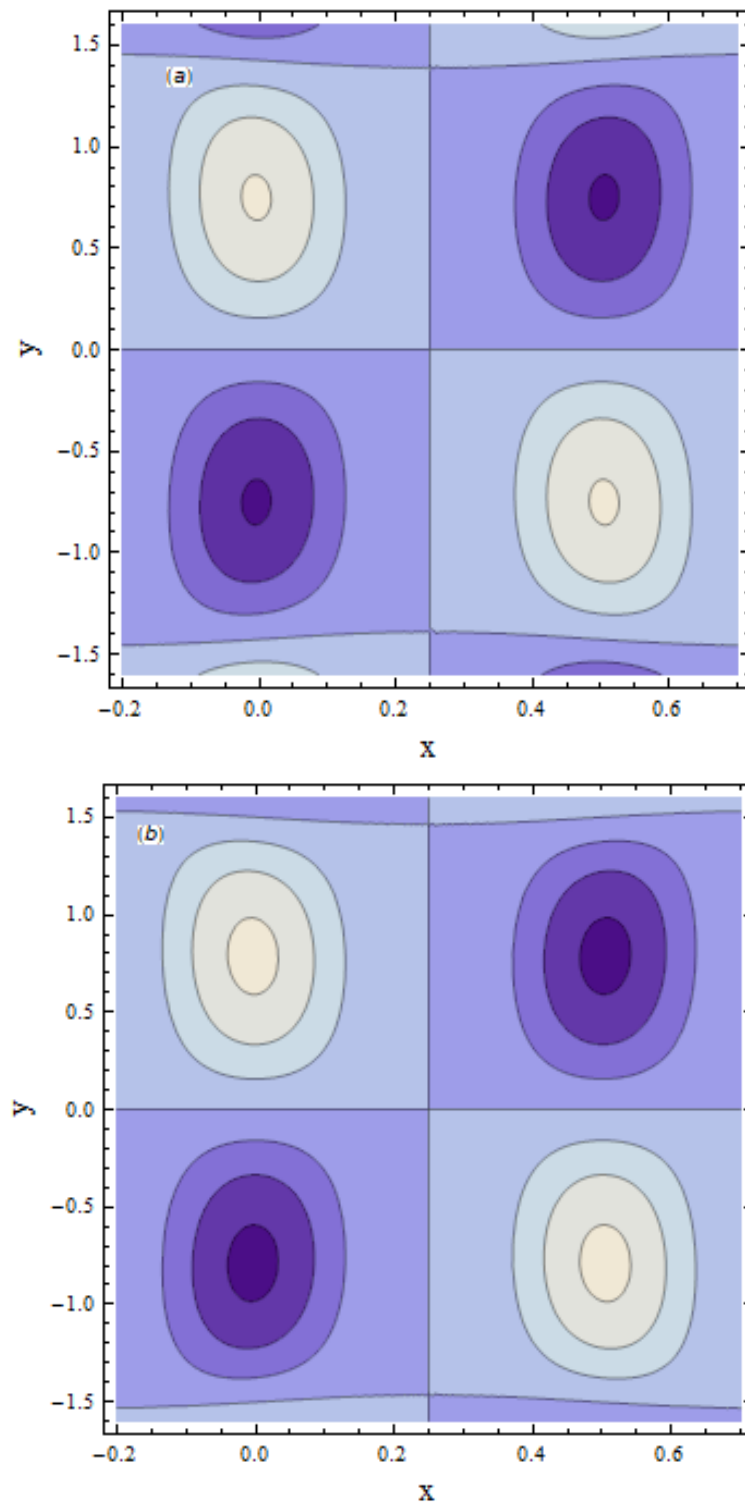


Figure 23. ψ variation when (a) $We = 0.1$ and (b) $We = 0.2$.

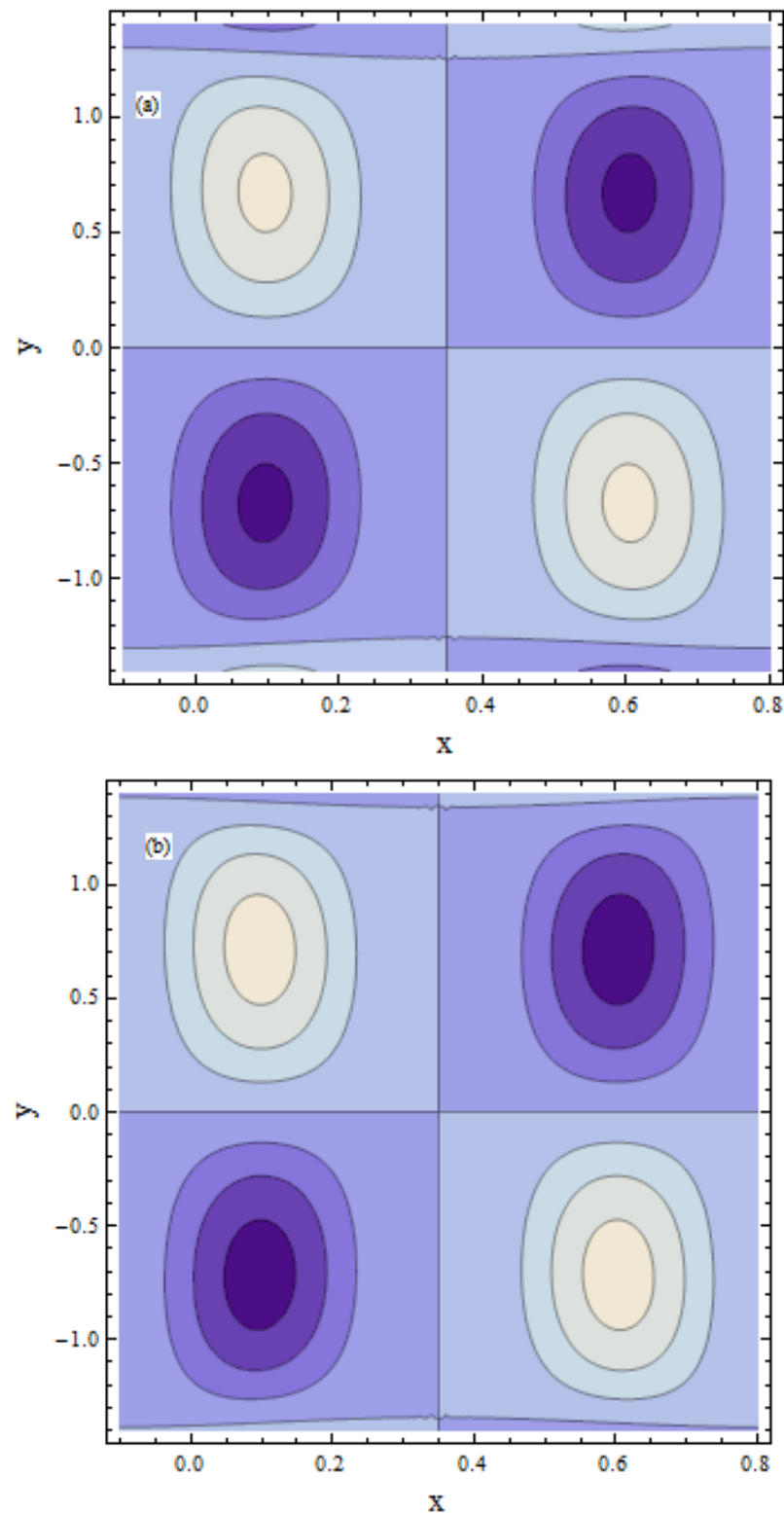


Figure 24. ψ variation when (a) $M = 0.3$ and (b) $M = 0.7$.

5. Conclusions

The effects of motile gyrotactic micro-organisms on the bioconvection peristaltic flow of a nanofluid were studied. The non-Newtonian Carreau–Yasuda model was used in this study. The slip conditions impose on the elastic channel walls. The impacts of joule heating, viscous dissipation, and thermal radiation were also taken into account. The governing problem was solved numerically. The velocity of the fluid increases with

increments in the velocity slip (β_1) and thermal Grashof (Gr) variables. The bioconvection Rayleigh (Gf) and Peclet (Pe) numbers have an inverse behavior on velocity. Temperature increases via Brownian motion (Nb) and the Brinkmann number (Br). The behaviors of the radiation variable (Rn) and the buoyancy ratio parameter (Gc) on temperature are reversed. The motile micro-organisms decrease via the bioconvection Peclet number (Pe) and thermophoresis (Nb) variable. The rate of heat transfer increases via the Grashof number (Gr) and the bioconvection Peclet parameter (Pe). The concentration declines via the bioconvection Peclet number (Pe). The results of Hayat et al. [13] are recovered when $(Gr, Gc, Gf, We, Rn) \rightarrow 0$.

Author Contributions: Conceptualization, Z.N. and H.Y.; methodology, Z.N.; software, Z.N.; validation, Z.N. and H.Y.; formal analysis, Z.N. and H.Y.; investigation, Z.N. and H.Y.; writing—original draft preparation, Z.N.; writing—review and editing, H.Y.; visualization, Z.N.; funding acquisition, H.Y. All authors have read and agreed to the published version of the manuscript.

Funding: This work was supported by the Deanship of Scientific Research, the Vice Presidency for Graduate Studies and Scientific Research, King Faisal University, Saudi Arabia (Grant No. 2478).

Institutional Review Board Statement: Not applicable.

Informed Consent Statement: Not applicable.

Data Availability Statement: Not applicable.

Conflicts of Interest: The authors declare no conflict of interest.

Nomenclature

(x,y)	Cartesian co-ordinates
a	wave amplitude
c	wave speed
p	pressure
d	coefficient of viscous damping
n	power law index
C	concentration
(u,v)	velocity components
t	time
d_1	half channel width
g	gravitational acceleration
k	thermal conductivity
T	temperature
Wc	maximum cell swimming speed
Greek symbols	
α	thermal diffusivity
ρ	density, kg/m^3
σ	electric conductions
Γ	material constant
σ	electric conductions
λ	wave length
δ	wave number
$(\beta_1, \beta_2, \beta_3)$	slip parameters
ψ	stream function

References

1. Latham, T. Fluid motion in a peristaltic pump. Master's Thesis, Massachusetts Institute of Technology, Cambridge, UK, 1966.
2. Shapiro, A.H.; Jaffrin, M.Y.; Weinberg, S.L. Peristaltic pumping with long wavelength at low Reynolds number. *J. Fluid Mech.* **1969**, *37*, 799–825. [[CrossRef](#)]
3. Mekheimer, K.S. Effect of the induced magnetic field on peristaltic flow of a couple stress fluid. *Phys. Lett. A* **2008**, *372*, 4271–4278. [[CrossRef](#)]

4. Ali, N.; Sajid, M.; Javed, T.; Abbas, Z. Heat transfer analysis of peristaltic flow in a curved channel. *Int. J. Heat Mass Transf.* **2010**, *53*, 3319–3325. [[CrossRef](#)]
5. Mustafa, M.; Hina, S.; Hayat, T.; Alsaedi, A. Influence of wall properties on the peristaltic flow of a nanofluid: Analytic and numerical solutions. *Int. J. Heat Mass Transf.* **2012**, *55*, 4871–4877. [[CrossRef](#)]
6. Hayat, T.; Iqbal, M.; Yasmin, H.; Alsaadi, F.E.; Gao, H. Simultaneous effects of Hall and convective conditions on peristaltic flow of couple-stress fluid in an inclined asymmetric channel. *Pramana* **2015**, *85*, 125–148. [[CrossRef](#)]
7. Sinnott, M.D.; Cleary, P.W.; Harrison, S.M. Peristaltic transport of a particulate suspension in the small intestine. *Appl. Math. Model.* **2017**, *44*, 143–159. [[CrossRef](#)]
8. Yasmin, H.; Iqbal, N.; Tanveer, A. Engineering applications of peristaltic fluid flow with hall current, thermal deposition and convective conditions. *Mathematics* **2020**, *8*, 1710. [[CrossRef](#)]
9. Nisar, Z.; Hayat, T.; Alsaedi, A.; Ahmad, B. Significance of activation energy in radiative peristaltic transport of Eyring-Powell nanofluid. *Int. Commun. Heat Mass Transf.* **2020**, *116*, 104655. [[CrossRef](#)]
10. Yasmin, H.; Iqbal, N.; Hussain, A. Convective heat/mass transfer analysis on Johnson-Segalman fluid in a symmetric curved channel with peristalsis: Engineering applications. *Symmetry* **2020**, *12*, 1475. [[CrossRef](#)]
11. Hina, S.; Kayani, S.M.; Mustafa, M. Aiding or opposing electro-osmotic flow of Carreau-Yasuda nanofluid induced by peristaltic waves using Buongiorno model. *Waves Random Complex Media* **2022**, 1–17. [[CrossRef](#)]
12. Abbasi, F.M.; Shehzad, S.A. Magnetized peristaltic transportation of boron-nitride and ethylene-glycol nanofluid through a curved channel. *Chem. Phys. Lett.* **2022**, *803*, 139860.
13. Hayat, T.; Nisar, Z.; Ahmad, B.; Yasmin, H. Simultaneous effects of slip and wall properties on MHD peristaltic motion of nanofluid with Joule heating. *J. Magn. Magn. Mater.* **2015**, *395*, 48–58. [[CrossRef](#)]
14. Hayat, T.; Nisar, Z.; Yasmin, H.; Alsaedi, A. Peristaltic transport of nanofluid in a compliant wall channel with convective conditions and thermal radiation. *J. Mol. Liq.* **2016**, *220*, 448–453. [[CrossRef](#)]
15. Rafiq, M.; Sajid, M.; Alhazmi, S.E.; Khan, M.I.; El-Zahar, E.R. MHD electroosmotic peristaltic flow of Jeffrey nanofluid with slip conditions and chemical reaction. *Alex. Eng. J.* **2022**, *61*, 9977–9992. [[CrossRef](#)]
16. Choi, S.U.S. *Enhancing Thermal Conductivity of Fluids with Nanoparticles*; Siginer, D., Wang, H., Eds.; Developments and Applications of Non-Newtonian Flows; ASME FE Argonne National Laboratory: Argonne, IL, USA, 1995; Volume 231, pp. 99–105.
17. Buongiorno, J.D. Convective transport in nanofluids. *ASME J. Heat Transf.* **2006**, *128*, 240–250. [[CrossRef](#)]
18. Tsai, C.Y.; Chien, H.T.; Ding, P.P.; Chan, B.; Luh, T.Y.; Chen, P.H. Effect of structural character of gold nanoparticles in nanofluid on heat pipe thermal performance. *Mater. Lett.* **2004**, *58*, 1461–1465. [[CrossRef](#)]
19. Li, Y.; Tung, S.; Schneider, E.; Xi, S. A review on development of nanofluid preparation and characterization. *Powd. Techn.* **2009**, *196*, 89–101. [[CrossRef](#)]
20. Yan, Q.; Lu, J.; Ni, X.W. Measurement of the Velocities of Nanoparticles in Flowing Nanofluids using the Zero-Crossing Laser Speckle Method. *Chin. Phys. Lett.* **2012**, *29*, 044207. [[CrossRef](#)]
21. Abbasi, F.M.; Hayat, T.; Ahmad, B. Peristaltic transport of copper-water nanofluid saturating porous medium. *Physica E* **2015**, *67*, 47–53. [[CrossRef](#)]
22. Akram, S.; Afzal, Q.; Aly, E.H. Half-breed effects of thermal and concentration convection of peristaltic pseudoplastic nanofluid in a tapered channel with induced magnetic field. *Case Stud. Therm. Eng.* **2020**, *22*, 100775. [[CrossRef](#)]
23. Bhatti, M.M.; Abdelsalam, S.I. Bio-inspired peristaltic propulsion of hybrid nanofluid flow with Tantalum (Ta) and Gold (Au) nanoparticles under magnetic effects. *Waves Random Complex Media* **2021**, 1–26. [[CrossRef](#)]
24. Alsaedi, A.; Nisar, Z.; Hayat, T.; Ahmad, B. Analysis of mixed convection and hall current for MHD peristaltic transport of nanofluid with compliant wall. *Int. Commun. Heat Mass Transf.* **2021**, *121*, 105121. [[CrossRef](#)]
25. Abbasi, F.M.; Zahid, U.M.; Akbar, Y.; Saba, B.; Hamida, M.B. Thermodynamic analysis of electroosmosis regulated peristaltic motion of Fe 3 O 4-Cu/H 2 O hybrid nanofluid. *Int. J. Modern Phys. B* **2022**, *36*, 2250060. [[CrossRef](#)]
26. Nisar, Z.; Hayat, T.; Alsaedi, A.; Ahmad, B. Mathematical modeling for peristalsis of couple stress nanofluid. *Math. Meth. Appl. Sci.* **2022**, 1–19. [[CrossRef](#)]
27. Hussain, A.; Wang, J.; Akbar, Y.; Shah, R. Enhanced thermal effectiveness for electroosmosis modulated peristaltic flow of modified hybrid nanofluid with chemical reactions. *Sci. Rep.* **2022**, *12*, 13756. [[CrossRef](#)]
28. Yasmin, H.; Giwa, S.O.; Noor, S.; Sharifpur, M. Experimental exploration of hybrid nanofluids as energy-efficient fluids in solar and thermal energy storage applications. *Nanomaterials* **2023**, *13*, 278. [[CrossRef](#)] [[PubMed](#)]
29. Singh, K.R.B.; Nayak, V.; Singh, R.P. Introduction to bionanomaterials: An overview. In *Bionanomaterials Fundamentals and Biomedical Applications*; IOP Publishing, Ltd.: Bristol, UK, 2021; pp. 1–21.
30. Jeevanandam, J.; Ling, J.K.U.; Barhoum, A.; Chan, Y.S.; Danquah, M.K. Bionanomaterials: Definitions, Sources, Types, Properties, Toxicity, And Regulations, Fundamentals of Bionanomaterials. *Micro Nano Technol.* **2022**, *15*, 1–29.
31. Hayat, T.; Abbasi, F.M.; Alsaedi, A.; Alsaadi, F. Hall and Ohmic heating effects on the peristaltic transport of a Carreau-Yasuda fluid in an asymmetric channel. *Z. Naturforschung A* **2014**, *69*, 43–51. [[CrossRef](#)]
32. Kayani, S.M.; Hina, S.; Mustafa, M. A new model and analysis for peristalsis of Carreau-Yasuda (CY) nanofluid subject to wall properties. *Arab. J. Sci. Eng.* **2020**, *45*, 5179–5190. [[CrossRef](#)]
33. Khan, M.I.; Alzahrani, F.; Hobiny, A.; Ali, Z. Estimation of entropy generation in Carreau-Yasuda fluid flow using chemical reaction with activation energy. *J. Mater. Res. Techn.* **2020**, *9*, 9951–9964. [[CrossRef](#)]

34. Nisar, Z.; Hayat, T.; Alsaedi, A.; Momani, S. Peristaltic flow of chemically reactive Carreau-Yasuda nanofluid with modified Darcy's expression. *Mater. Today Commun.* **2022**, *33*, 104532. [[CrossRef](#)]
35. Iqbal, J.; Abbasi, F.M. Analysis of entropy generation for Magnetohydrodynamics peristaltic motion of Carreau-Yasuda nanofluid through a curved channel with variable thermal conductivity and Joule heating. *Waves Random Complex Media* **2022**, 1–20. [[CrossRef](#)]
36. Pedley, T.J.; Hill, N.A.; Kessler, J.O. The growth of bioconvection patterns in a uniform suspension of gyrotactic micro-organisms. *J. Fluid Mech.* **1988**, *195*, 223–237. [[CrossRef](#)] [[PubMed](#)]
37. Waqas, H.; Khan, S.U.; Hassan, M.; Bhatti, M.M.; Imran, M. Analysis on the bioconvection flow of modified second-grade nanofluid containing gyrotactic microorganisms and nanoparticles. *J. Mol. Liq.* **2019**, *291*, 111231. [[CrossRef](#)]
38. Rao, M.; Gangadhar, K.; Chamkha, A.J.; Surekha, P. Bioconvection in a convectonal nanofluid flow containing gyrotactic microorganisms over an isothermal vertical cone embedded in a porous surface with chemical reactive species. *Arab. J. Sci. Eng.* **2021**, *46*, 2493–2503. [[CrossRef](#)]
39. Hayat, T.; Nisar, Z.; Alsaedi, A. Bioconvection and Hall current analysis for peristalsis of nanofluid. *Int. Commun. Heat Mass Transf.* **2021**, *129*, 105693. [[CrossRef](#)]
40. Hussein, S.A.; Ahmed, S.E.; Arafa, A.A. Electrokinetic peristaltic bioconvective Jeffrey nanofluid flow with activation energy for binary chemical reaction, radiation and variable fluid properties. *Z. Angew. Math. Mech.* **2022**, *103*, e202200284. [[CrossRef](#)]
41. Akbar, Y.; Huang, S. Enhanced thermal effectiveness for electrokinetically driven peristaltic flow of motile gyrotactic microorganisms in a thermally radiative Powell Eyring nanofluid flow with mass transfer. *Chem. Phys. Lett.* **2022**, *808*, 140120. [[CrossRef](#)]
42. Avramenko, A.; Kovetska, Y.Y.; Shevchuk, I.V. Lorenz approach for analysis of bioconvection instability of gyrotactic motile microorganisms. *Chaos Solit. Fractals* **2023**, *166*, 112957. [[CrossRef](#)]
43. Gad-el-Hak, M. Compliant coatings: The simpler alternative. *Exp. Therm. Fluid Sci.* **1998**, *16*, 141–156. [[CrossRef](#)]
44. Gad-El-Hak, M. Drag Reduction Using Compliant Walls. In *Flow Past Highly Compliant Boundaries and in Collapsible Tubes. Fluid Mechanics and Its Applications*; Carpenter, P.W., Pedley, T.J., Eds.; Springer: Dordrecht, The Netherlands, 2003; p. 72.
45. Kramer, M.O. Boundary-layer stabilization by distributed damping. *J. Aeronaut. Sci.* **1957**, *24*, 459–460.

Disclaimer/Publisher's Note: The statements, opinions and data contained in all publications are solely those of the individual author(s) and contributor(s) and not of MDPI and/or the editor(s). MDPI and/or the editor(s) disclaim responsibility for any injury to people or property resulting from any ideas, methods, instructions or products referred to in the content.